Statistical modeling of biogenically enhanced permeability in tight reservoir rock

Amy I. Hsieh [ab,*], Diana M. Allen [b], James A. MacEachern [a]

[a] Applied Research in Ichnology and Sedimentology (ARISE) Group, Department of Earth Sciences, Simon Fraser University, Burnaby, British Columbia, Canada V5A 1S6
[b] Groundwater Resources Research Group (GRRG), Department of Earth Sciences, Simon Fraser University, Burnaby, British Columbia, Canada V5A 1S6

[*] Corresponding author. Tel: +1 778 782 5429
Email addresses: aih2@sfu.ca (A.I. Hsieh), dallen@sfu.ca (D.M. Allen), jmaceach@sfu.ca (J.A. MacEachern).

This paper was published in Marine and Petroleum Geology 65 (2015) 114-125.
http://dx.doi.org/10.1016/j.marpetgeo.2015.04.005

Highlights

1. Hydrofacies (HF) are defined on the basis of sedimentary and ichnologic features.

2. Markov chain analysis is used to assess the effect of grain size vs. HF on k_{max}.

3. The volumetric proportions of k_{max} show a 15% correlation with grain size.

4. The volumetric proportions of k_{max} show a 97% correlation with HF.

Abstract

Bioturbation is generally perceived to be detrimental to bulk permeability by reducing primary grain sorting, homogenizing sediment, and introducing mud as burrow linings and feces. Recent studies show, however, that some ichnogenera and biogenic fabrics serves to increase porosity and permeability. In tight hydrocarbon reservoirs, subtle changes in sand and silt distributions, such as may be generated by bioturbation, can greatly affect the resulting porosity and permeability distribution. Despite this, permeability across unfractured sedimentary reservoirs is commonly assessed solely on the basis of average grain size. This study of the Lower Cretaceous Viking Fm integrates sedimentary and ichnologic features to define recurring "hydrofacies" that possess distinct permeability grades. Grain size, lithology, bioturbation index, and trace fossil suites were described from a cored section of well 14-30-22-16W4. The k_{max} values from small plugs and full-diameter core samples were used to represent each hydrofacies. Hydrofacies were qualitatively defined at the bed/bedset scale, based on sedimentary, ichnological and permeability attributes, all of which affect flow pathways in heterolithic facies. The Markov chain method was employed to compare the vertical transitions of permeability (k_{max}) within a borehole against grain size and hydrofacies at the bed to bedset scale. This provided an intuitive framework for interpreting facies relationships such as coarsening-upwards successions. The results show that in the studied core, grain size only correlates to permeability in homogeneous rock units. The transiograms show that the volumetric proportions of different k_{max} classes show a 15% correlation with grain size, compared to a 97% correlation with the hydrofacies, indicating that variations in permeability down the well are strongly related to variations in the hydrofacies. The hydrofacies approach potentially can be used as a conceptual

framework for the spatial modeling of permeability in tight hydrocarbon reservoirs, where grain size may not be the primary factor on permeability distributions.

Keywords: Bioturbation; hydrofacies; statistical modeling; Markov chain; permeability

1. Introduction

The storage capacity and productivity of a reservoir are determined by its porosity and permeability. Permeability is also an important factor that controls reservoir response during enhanced recovery. Correspondingly, understanding and projecting variations in porosity and permeability within a reservoir are vital to maximizing the acquisition of the resource. Recently, there has been considerable interest in recovering hydrocarbons from marginal (generally lower-quality) reservoirs using horizontal drilling techniques and fracturing, particularly in areas prone to light oil. The so-called "Tight Oil" play of the Viking Formation in east-central Alberta and west-central Saskatchewan is one example. "Tight" reservoirs are characterized by permeabilities that range from 0.01-0.1 mD (Spencer, 1989; Holditch, 2006; Clarkson and Pedersen, 2010). In such reservoirs, subtle changes in the distribution of sedimentary media, such as are generated by bioturbation, can greatly affect the porosity and permeability distribution of the facies.

Bioturbation remains an under-appreciated mechanism by which porosity and permeability of a sedimentary facies are modified (cf. Pemberton and Gingras, 2005). Even when considered, bioturbation is generally perceived to be detrimental to bulk permeability, through reduction of primary grain sorting, homogenization of the sediment, and introduction of mud through linings, biogenic deposits, and feces (Qi, 1998; Dornbos et al., 2000; Qi et al., 2000; McDowell et al., 2001; Pemberton and Gingras, 2005; Tonkin et al., 2010; Lemiski et al., 2011;

La Croix et al., 2013). Recent studies have shown, however, that several ichnogenera and their associated biogenic fabrics are capable of increasing a reservoir rock's porosity and permeability (Gingras et al., 2004; Pemberton and Gingras, 2005; Hovikoski et al., 2007; Volkenborn et al., 2007; Cunningham et al., 2009; Tonkin et al., 2010; Lemiski et al., 2011; Gingras et al., 2012; La Croix et al., 2013; Knaust, 2014). Ichnogenera that form branching burrow networks can create flow pathways in otherwise less permeable units where the burrow fills consist of coarser grains and better-connected intergranular pore space relative to the surrounding matrix (Figure 1; Gingras et al., 2004; Pemberton and Gingras, 2005; Lemiski et al., 2011; Gingras et al., 2012; La Croix et al., 2013). Additionally, burrows are capable of increasing vertical permeability in laminated sedimentary rocks, where horizontal permeability otherwise tends to dominate (Gingras et al., 2012). Burrow fills also may undergo diagenetic changes that may lead to higher permeability than that of the surrounding matrix (Pemberton and Gingras, 2005; Tonkin et al., 2010; Gingras et al., 2012).

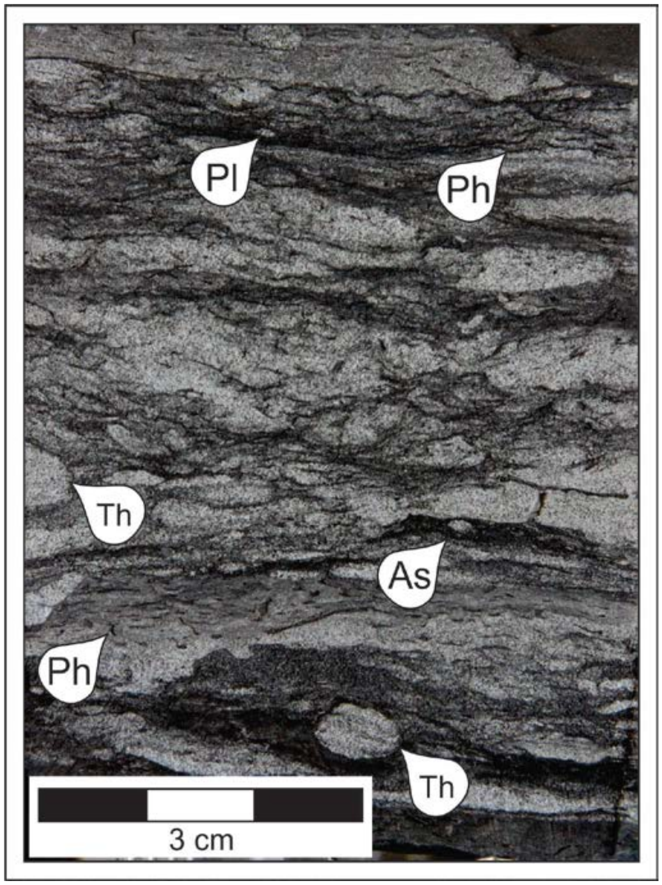

Figure 1 Sand-filled trace fossils, such as *Thalassinoides* (Th) and *Planolites* (Pl) create potential flow paths in an otherwise low-permeability unit. Mud-filled traces are dominated by *Phycosiphon* (Ph).

Despite this, permeability across unfractured sedimentary reservoirs is commonly assessed solely on the basis of grain size (e.g. lithostratigraphic units). By contrast, this paper proposes the use of "hydrofacies" (HF) in reservoir characterization. A hydrofacies is defined herein as a recurring sedimentary facies possessing a distinct permeability grade generated by a combination of sedimentological and ichnological characteristics. Such a hydrofacies takes into account the lithology, textural characteristics, physical and biogenic fabric, the presence and distribution of trace fossils, and the expression of burrow fill(s), all of which serve to affect permeable flow pathways (vertically and laterally) in heterolithic facies. The Markov chain approach proposed in this paper is used to compare vertical transitions in permeability within a borehole with transitions in a) grain size, and b) hydrofacies at the bed to bedset scale, in order to determine which variable best reflects the observed permeability variations.

2. Geologic Setting

The Lower Cretaceous (Upper Albian) Viking Formation is a prolific oil- and gas-producing interval that was deposited in the Western Canada foreland basin during a period of active tectonism and eustatic sea level fluctuations. During Viking deposition, a shallow epicontinental seaway extended from the Arctic Ocean to the Gulf of Mexico (Figure 2; Williams and Stelck, 1975; Caldwell, 1984; Walker, 1990; Reinson et al., 1994), into which was deposited a complex succession of siliciclastics, dominated by mudstones, heterolithic bedsets of sandstone and shale, and sandstones, with minor conglomerates.

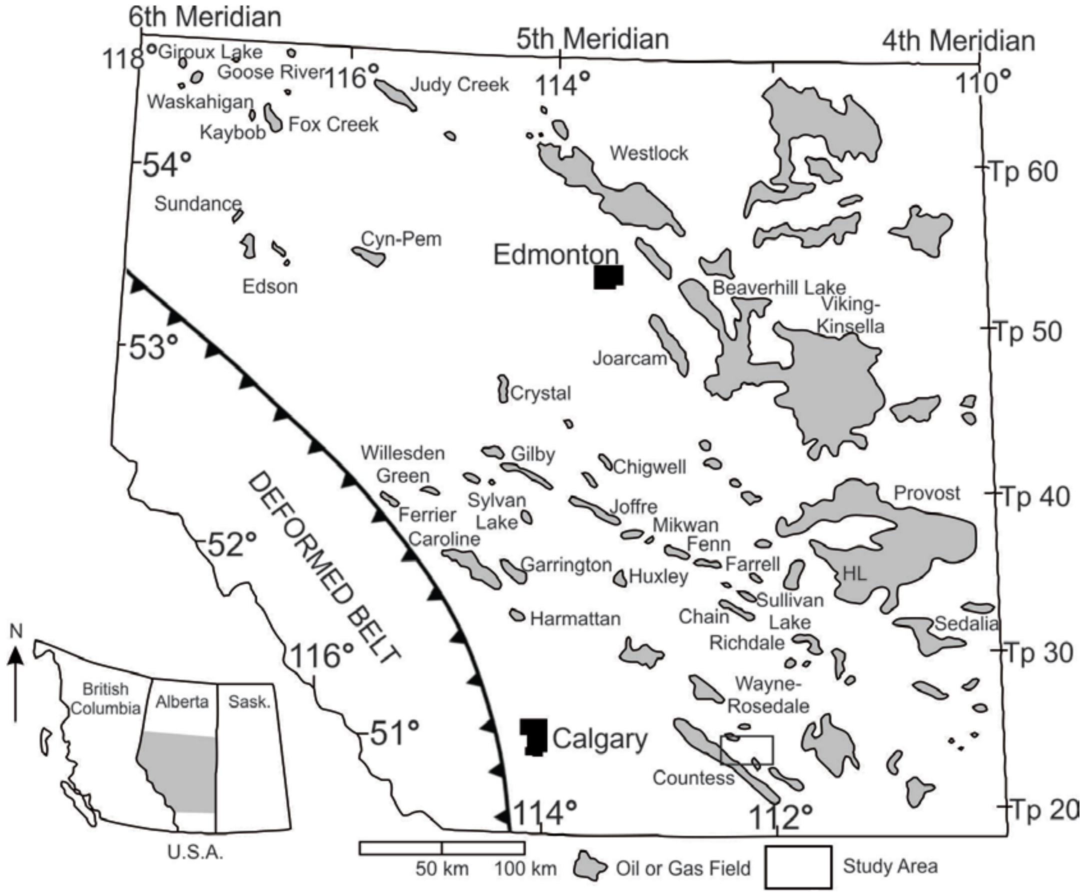

Figure 2 Map showing the major hydrocarbon-producing fields of the Viking Formation in Alberta (MacEachern et al., 1999).

The Viking Formation stratigraphically overlies the Joli Fou Formation and underlies the Westgate Formation (Figure 3; Stelck, 1958). It is generally regarded to be roughly equivalent to the Paddy Member of the Peace River Formation of northwestern Alberta (Leckie et al., 1990), and the Bow Island Formation of southern Alberta and southwestern Saskatchewan (Figure 3; Stelck and Koke, 1987; Raychaudhuri and Pemberton, 1992). While the Viking sediments only range from 15 to 30 m in thickness, they are discontinuity-bound and depositionally complex, resulting in sedimentary successions, facies, and geometries that are challenging to characterize and correlate (e.g. Pattison, 1991; Reinson et al., 1994; Walker, 1995; Burton and Walker, 1999).

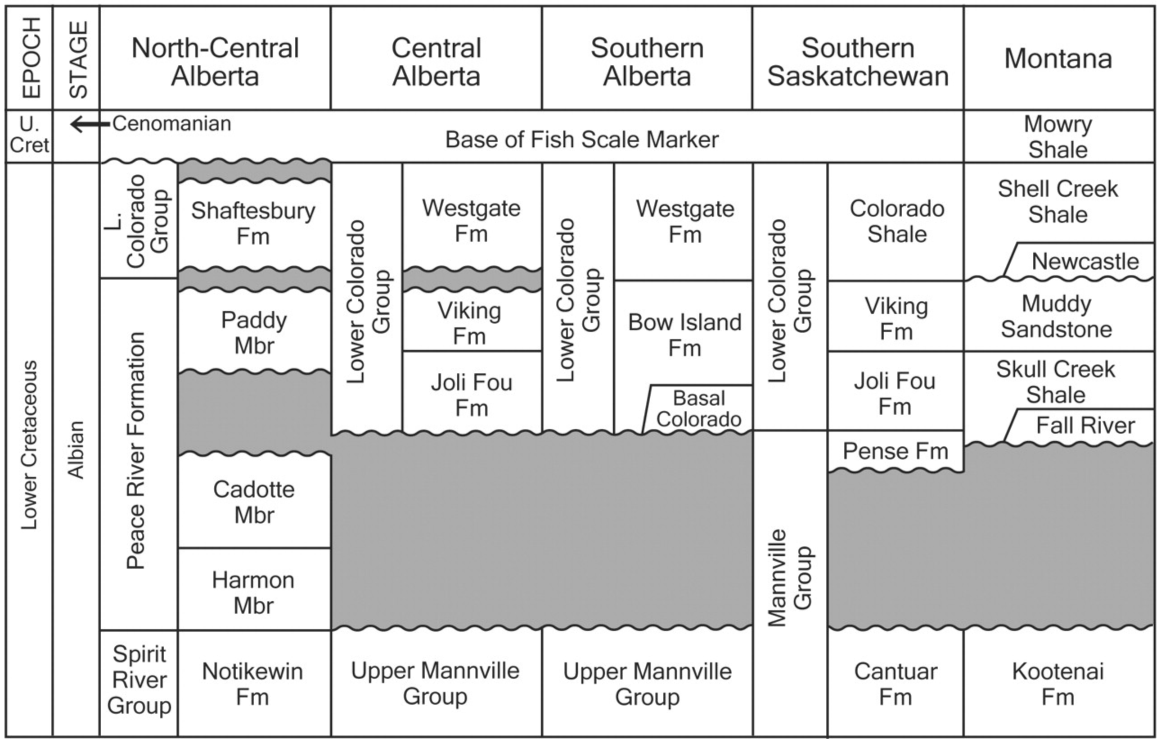

Figure 3 Stratigraphic correlation diagram of the Viking Formation in central Alberta showing the overlying Westgate Formation, underlying Joli Fou Formation, as well as its stratigraphic equivalents, the Paddy Member and Bow Island Formation (MacEachern et al., 1999).

The Late Albian (Lower Cretaceous) Viking Formation comprises a siliciclastic succession consisting of interstratified mudstones, sandstones and rare conglomerates, mainly reflecting shoreface, delta and estuarine valley deposits. These clastics were supplied from the rising Cordillera in the west and reflect northward and eastward progradation of environments into the Alberta foreland basin. The Viking Formation overlies marine shale of the Joli Fou Formation and is capped by marine shale of the Westgate Formation (Fig. 3). The stratigraphic relationships were addressed by the work of Stelck (1958), Glaister (1959), McGookey et al.

(1972), Weimer (1984), Cobban and Kennedy (1989), Stelck and Leckie (1990), Bloch et al. (1993), Caldwell et al. (1993), and Obradovich (1993).

The Viking Formation is internally complex stratigraphically, and characterized by numerous internal discontinuities. Beaumont (1984), Boreen and Walker (1991), Pattison (1991), Posamentier and Chamberlain (1993), Reinson et al. (1994), Walker (1995), Burton and Walker (1999), and MacEachern et al. (1999), among others, have attempted to provide allostratigraphic and sequence stratigraphic assessments of the Viking, with varying levels of success. Viking Formation discontinuities have been linked to the global changes of sea level outlined in Kauffman (1977), Vail et al. (1977), Weimer (1984), and Haq et al. (1987). A cored interval of the Viking Formation from the Verger Field was selected for this study because it exhibits stacked parasequences characterized by the interstratification of impermeable and permeable beds with variable but locally pervasive bioturbation.

3. Geostatistics

In this study, the transition probability method is used to model bioturbated, heterogeneous sedimentary media. The transition probability method is a modified form of indicator kriging that assumes the type of sediment that *will* be deposited in a stratigraphic succession depends solely upon what is currently being deposited in the present environment and not on the rock types deposited in past environments (Jones et al., 2002). For example, in a prograding shoreface environment, one would expect to find a gradual upward-coarsening succession of facies. If the rock type observed is fine-grained parallel laminated sandstone of the middle shoreface, the next unit to be deposited is more likely to be coarser-grained cross-stratified sandstone of the upper shoreface, regardless of what rock type was deposited *before* the fine-grained parallel laminated sandstone. In terms of spatial distributions, the probability of the occurrence of a class is dependent on the nearest occurrence of another class over a specified lag interval. The probability of class 1 passing into class 2 can be defined by:

$$p_{12}h_{\Phi} = Pr\{(class\ 2\ occurs\ at\ x + h_{\Phi})|(class\ 1\ occurs\ at\ x)\} \qquad (1)$$

where h_{Φ} represents the lag distance in the direction Φ (Carle, 1999).

The spatial correlation among different sedimentary facies can be calculated using a Markov chain analysis; a mathematical model that transitions from one state to another between a fixed number of possible discrete states (Carle, 1999). For example, a succession of sedimentary facies may be characterized by a preferred tendency for sediment A to be deposited after sediment B, but not sediment C; therefore, the spatial occurrence of sediment A may be dependent on the pre-existence of sediment B but independent of sediment C (Li et al., 2005). Additionally, if sediments A, B, and C tend to be deposited upwards as a sequence ABC, this asymmetric relationship also can be characterized using Markov chain analysis (Li et al., 2005).

The Markov chain is described as follows: There is a set of classes, $S = \{s_1, s_2, \ldots, s_r\}$, which pass sequentially from one to another in steps. The probability of class s_1 moving to class s_2 is represented by p_{12}, otherwise known as the transitional probability from s_1 to s_2. If the transition remains in the same class s_1, it is denoted by the probability p_{11} (Grinstead and Snell, 1997). For example, Carle (1999) assessed the transition probabilities down a well log using an embedded analysis of the Markov chain with respect to a matrix of vertical transitions from one discrete sedimentary facies to another. In that study, an embedded Markov chain analysis of a vertical succession was defined by three facies (A, B, and C) according to the following steps (Carle, 1999):

1. Disregard the lag or spatial dependency and relative thicknesses of the beds.
2. Log the embedded occurrences of A, B, and C down the borehole (e.g. ABCABACABCABABC).
3. Count the number of transitions from one state to another in a transition count matrix.

	A	**B**	**C**
A	-	5	1
B	2	-	3
C	3	0	-

   Self-transitions (e.g. from A to A) are unobservable in single or stacked beds, and are therefore null in the transition matrix.

4. Divide each transition count by the sum of the row, in order to find the embedded transition probabilities.

	A	**B**	**C**
A	-	0.833	0.167
B	0.4	-	0.6
C	1	0	-

   This final matrix shows the transition probabilities for each combination of units.

The Markov transition probability approach is generally useful for stratigraphically confined systems. As is clear from Walther's Law, genetic and predictable relationships exist for facies successions that occur between stratigraphic breaks, which are absent in facies separated by such breaks. Markov transition probability can be used to demonstrate the lack of correlatibility of facies across such stratigraphic breaks (Weissmann, 2005). Another advantage of using Markov chain models is that the approach assumes stratigraphic stationarity (statistical homogeneity; i.e. the mean and standard deviation do not change over time or space) across the modeled reservoir (Weissmann, 2005). In other words, by dividing the core into facies, the proportions and geometries of different facies within the environment are maintained. In a transgressive marine environment, for example, the proportion of fine-grained facies is higher than coarse-grained facies across the environment, and the probability of fine-grained facies being deposited is likewise greater. This ensures that a facies represented in the model is not a result of random variables, but rather is reflective of the character of the depositional conditions. Furthermore, the distribution of facies within the stratigraphic unit theoretically can be simulated, resulting in a quantifiable conceptual model that facilitates the interpretation of the reservoir's heterogeneity (Weissmann, 2005).

4. Methodology

4.1 Core Logging

Well 14-30-22-16W4 in the Verger Field contains core through the Viking Formation, and was selected for this study because it exhibits the interlayering of impermeable and permeable beds (e.g. mudstones and sandstones) that are thoroughly bioturbated in certain sections. All of the physical and biogenic features observed in the core, including lithology, grain size, bioturbation index (BI) and ichnological suites, were logged from the base to the top of the well using AppleCORE, a core-logging program that allows the user to record descriptive geological data and convert the data into a strip log (Figure 6).

4.2 Permeability Data

The permeability data for the well were obtained from AccuMap, an oil and gas mapping, data management and analysis software for companies operating in the Western Canadian Sedimentary Basin and Frontier areas (AccuMap IHS; accessed 06 February, 2013). The AccuMap data for well 14-30-22-16W4 include 44 horizontal permeability (k_{max}) values that were measured at discrete locations over the length of the core. Each k_{max} value was measured using both plug and full diameter samples from the core. At the bed/bedset scale, an average k_{max} value was calculated from the raw permeability data to represent each HF as described below. For the transition probability analysis, the k_{max} values were classed by increasing magnitudes in logarithmic scale (0.01, 0.1, 1, 10, and 100 mD) to enable comparison firstly between permeability and grain size, and secondly between permeability and HF.

4.3 Hydrofacies and Parameter Class Divisions

Hydrofacies (HF) were qualitatively defined at the bed/bedset scale based on distinct sedimentary, ichnological, and *potential* permeability attributes. The average grain sizes observed in the core were divided according to the Wentworth (1922) grain-size classification scale: clay, silt, lower fine-grained sand, upper fine-grained sand, and lower medium-grained sand. Bioturbation index (BI) reflects grades of bioturbation intensity, and were assigned values from 0 to 6, with 0 being unburrowed, and 6 being the most intensely burrowed (Figure 4; Reineck, 1963; Taylor and Goldring, 1993; Taylor et al., 2003). BI values of 6 (complete bioturbation) were not observed in the cored interval.

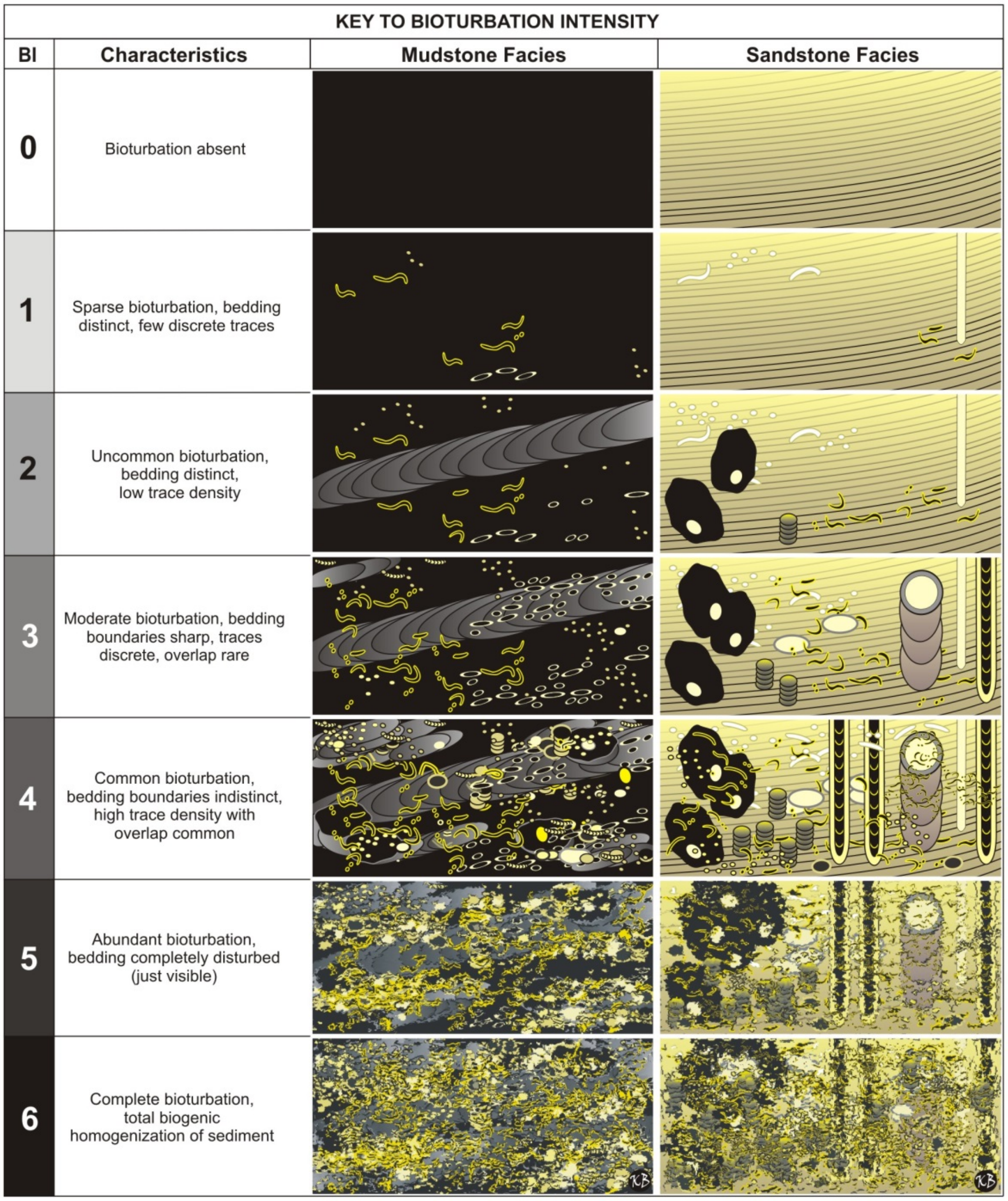

Figure 4 Schematic diagram of the bioturbation index (BI), modified from Reineck (1963), Taylor and Goldring (1993) and Taylor et al. (2003) by MacEachern and Bann (2008). Bioturbation grades correspond to: BI 0 = 0% bioturbation; BI 1 = 1-4% bioturbation; BI 2 = 5-30% bioturbation; BI 3 = 31-60% bioturbation; BI 4 = 61-90% bioturbation; BI 5 = 91-99% bioturbation; and BI 6 = 100%.

4.4 Transition Probability Analysis

The probabilities of each class transitioning to another were calculated using the Transition Probability Geostatistical Software (T-PROGS), developed by Carle (1999) within the Groundwater Modelling Software (GMS version 6.0, Copyright © 2013 Aquaveo). The transition probability matrices for grain size and HF were compared to that of k_{max}. The volumetric proportion is represented by the “sill”, where the transiogram reaches its limit at infinity lag distances (Figure 5). The mean lens thickness is represented by the distance at which the tangent line to the transiogram intersects the x- or lag-axis (Figure 5; Cahn et al., 1994). In a transition probability matrix, the self-transition curves start at a probability of one or 100% and decrease with increasing lag distances, whereas the off-diagonal curves start at a probability of zero (0%) and increase with lag distance (Carle, 1999).

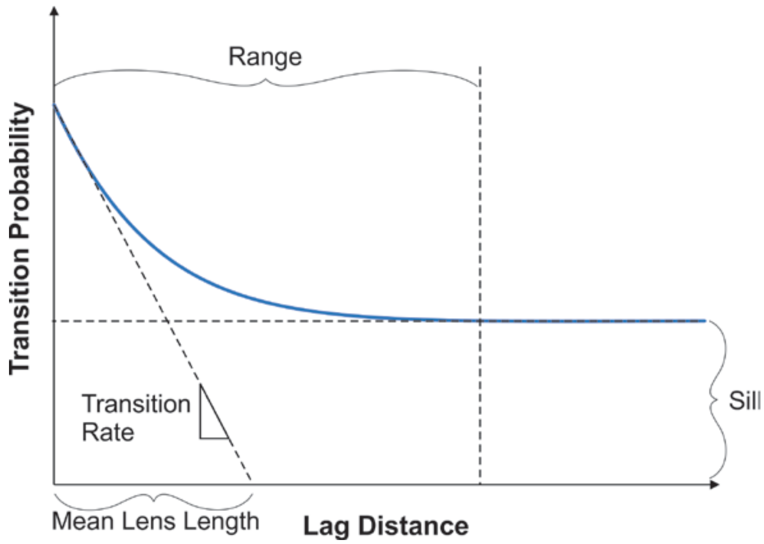

Figure 5 Example of a Markov chain transiogram. The transition probability value at which the Markov chain levels out is the "sill" and the lag distance at which the Markov chain reaches the sill is the "range". The transition rate is defined by the slope of the tangent line, and the mean lens length is the lag distance at which the tangent line intersects the x-axis.

5. Results and Discussion

5.1 Hydrofacies

Five hydrofacies were identified at the bed/bedset scale in the studied core (Table 1): bioturbated/non-bioturbated mudstone; bioturbated silty mudstone; bioturbated muddy sandstone; bioturbated sandstone; and sandstone. For the logged core, only plug permeability data were available for HF 4 and 5, and only full-diameter core permeability data were available for HF 2 and 3. The plug and full-diameter core analyses capture permeability at different scales. The plug permeability represents k at the bed scale, whereas full-diameter permeability analyses capture bulk permeability. In heterogeneous units, for example, the plug permeability may be biased towards coarser-grained more permeable units, while full diameter analyses capture the permeability of both coarse- and fine-grained units and is more representative of the overall permeability. Due to the paucity of data, however, the plug and full diameter permeability measurements are assumed to be equivalent. Additionally, because the plug samples only measure k_{max} in the horizontal direction, the horizontal k_{max} measured in the full diameter samples were used instead of $k_{vertical}$. The average permeability (k_{avg}) is calculated for HF 2, 3, and 5. For HF 4, only one permeability measurement was available, so that value (k_{max}) is assumed to be representative for all HF 4 at the bed/bedset scale. Permeability was not measured for any of the mudstone hydrofacies (HF 1); therefore, the geometric mean (geomean) of the range of mudstone permeabilities measured in other studies was used (e.g. Mesri and Olson, 1971; Long, 1979; Long and Hobbs, 1979; Nagaraj et al., 1994; Dewhurst et al., 1998, 1999; Yang and Aplin, 2007, 2010). Table 1 reports the average or representative k values for each HF.

Table 1 Bed/bedset scale hydrofacies descriptions. The calculated k_{ave} (mD) or representative k_{ave} based on previous studies for each HF are also reported.

Hydrofacies		Lithology	Grain Size	Sedimentary Structures	BI	Trace Fossils (in approximate order of decreasing abundance)	k_{ave} (mD)
1	Apparently structureless mudstone	Mudstone	Clay	Apparently structureless, sharp-based mudstone	Apparently low (BI 0-1) or high (BI 4-5) if bioturbation is present and observable	Rare *Chondrites* and *Planolites*	1.31E-04[a]
2	Bioturbated silty mudstone	Mudstone with moderate proportions of interstitial silt and sand	Lower to upper silt	No sedimentary structures observed	4-5	*Phycosiphon*, *Chondrites*, *Helminthopsis*, *Planolites*, *Asterosoma*, *Schaubcylindrichnus*, *Thalassinoides*, *Teichichnus*, *Zoophycos*, *Diplocraterion*, with rare *Rosselia* and fugichnia	0.35
3	Bioturbated muddy sandstone	Sandstone with moderate proportions of interstitial silt and clay	Lower fine- to upper fine-grained sand	No sedimentary structures observed	3-5	*Phycosiphon*, *Chondrites*, *Helminthopsis*, *Planolites*, *Asterosoma*, *Teichichnus*, *Schaubcylindrichnus*, *Zoophycos*, *Thalassinoides*, *Palaeophycus*, *Diplocraterion*, *Skolithos*, *Ophiomorpha*, *Rosselia*, *Rhizocorallium* and fugichnia	1.24
4	Bioturbated sandstone	Sandstone	Lower fine- to upper fine-grained sand	Apparently structureless	4-5	*Phycosiphon*, *Asterosoma*, and fugichnia	5.03[b]
5	Sandstone	Sandstone	Lower fine- to upper fine-grained sand	HCS or horizontal to low-angle (5°) planar parallel laminated or wave ripple laminated, sharp-based	0	Not observed	4.20

a Calculated geometric mean of values from the literature
b Only one value available for the core

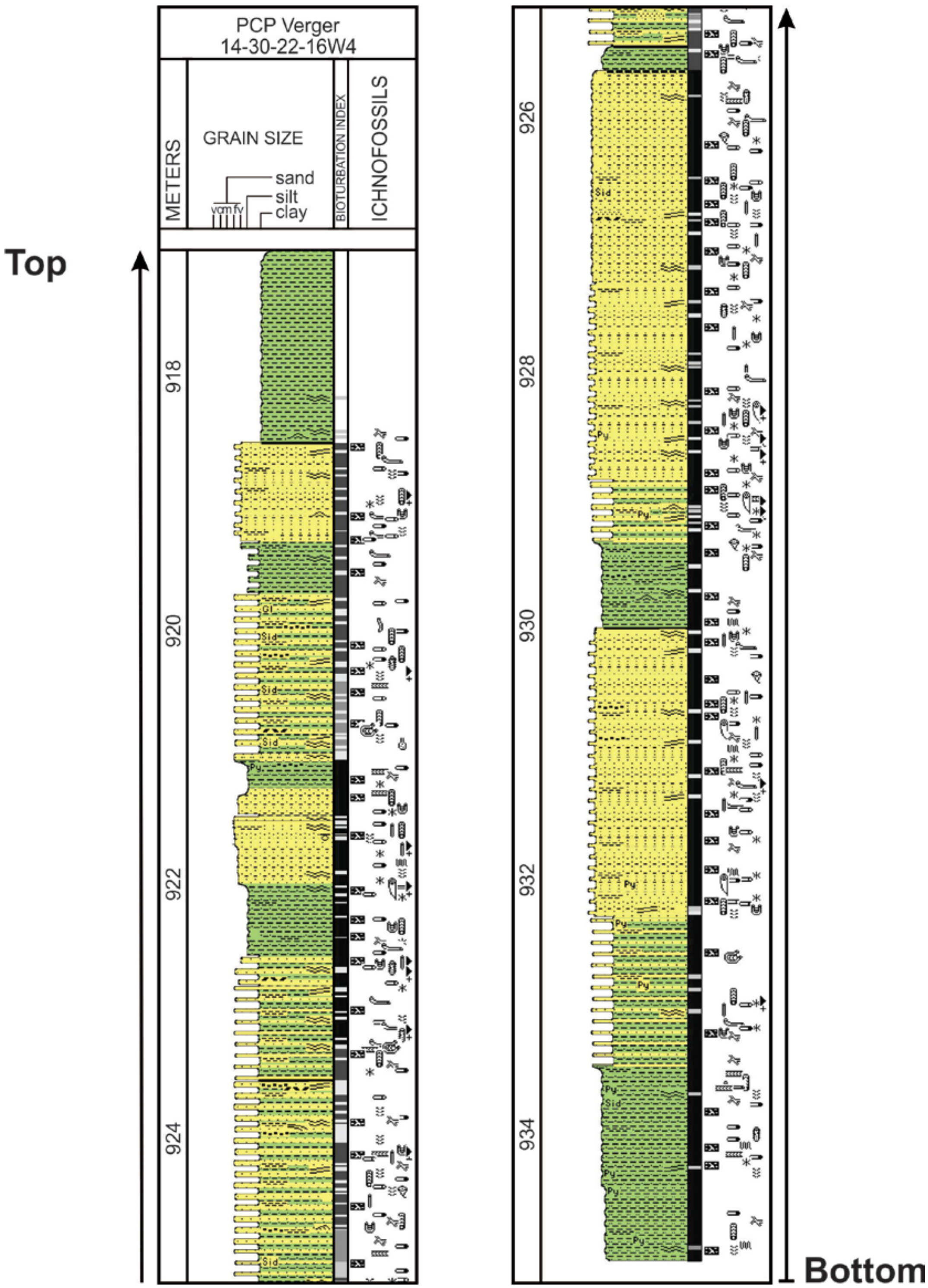
PCP Verger
14-30-22-16W4
METERS
GRAIN SIZE
sand
silt
clay
vcmfvf
BIOTURBATION INDEX
ICHNOFOSSILS
Top
Bottom
918
920
922
924
926
928
930
932
934

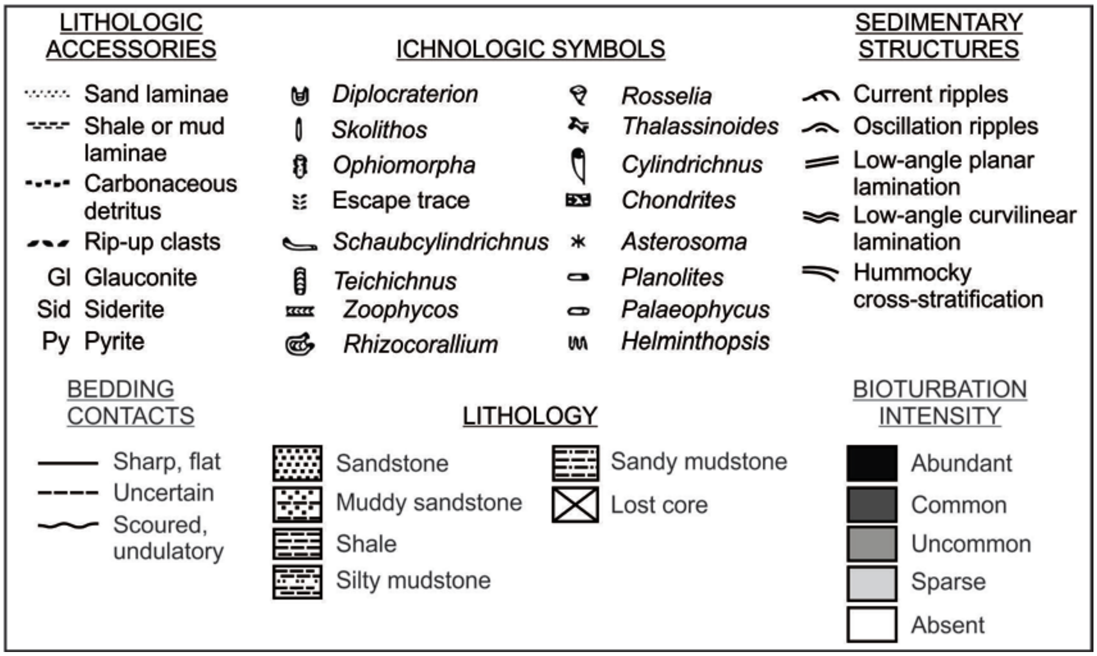

Figure 6 Core log of PCP Verger 14-30-22-16W4.

HF 1 encompasses apparently structureless, sharp-based mudstones (Figure 7). Bioturbation may appear absent (BI 0-1) owing to a homogeneously muddy matrix, but where interstitial silt and sand contents are slightly higher or burrows reflect sand or silt segregation from the matrix, bioturbation intensities may range from 4-5. Trace fossils in HF 1 include rare *Chondrites* and *Planolites*. The k_{ave} calculated from previous work is 1.31E-04 mD (cf. Mesri and Olson, 1971; Long, 1979; Long and Hobbs, 1979; Nagaraj et al., 1994; Dewhurst et al., 1998, 1999; Yang and Aplin, 2007, 2010).

HF 2 corresponds to bioturbated silty mudstone with moderate proportions of interstitial silt and sand (Figure 7). Primary stratification is not preserved. Bioturbation intensities are high (BI 4-5) with a diverse trace fossil suite consisting of *Phycosiphon, Chondrites, Helminthopsis, Planolites, Asterosoma, Schaubcylindrichnus,* *Thalassinoides, Teichichnus, Zoophycos, Diplocraterion,* with rare *Rosselia* and fugichnia, in order of approximate decreasing abundance. The k_{ave} value for HF 2 is 0.35 mD.

HF 3 is characterized by bioturbated muddy sandstones with moderate proportions of interstitial silt and clay (Figure 7). No primary sedimentary structures are preserved in HF 3 due to the high bioturbation intensities (BI 3-5). The diverse trace fossil suite, in order of approximate decreasing abundance, comprises *Phycosiphon, Chondrites, Helminthopsis, Planolites, Asterosoma, Teichichnus, Schaubcylindrichnus, Zoophycos, Thalassinoides, Palaeophycus, Diplocraterion, Skolithos, Ophiomorpha, Rosselia, Rhizocorallium* and fugichnia. The k_{ave} value for HF 3 is 1.24 mD.

HF 4 consists of sandstones with rare preserved primary sedimentary structures due to bioturbation (Figure 7). Bioturbation intensities range from BI 4-5, and the trace fossil suite includes isolated *Phycosiphon, Asterosoma,* and fugichnia. The representative k value for HF 4 is 5.03 mD.

HF 5 is composed of unburrowed (BI 0), well-sorted sandstones that are hummocky cross-stratified, horizontal to low-angle (5°) planar parallel laminated, or wave-ripple laminated (Figure 7). The k_{ave} value for HF 5 is 4.20 mD.

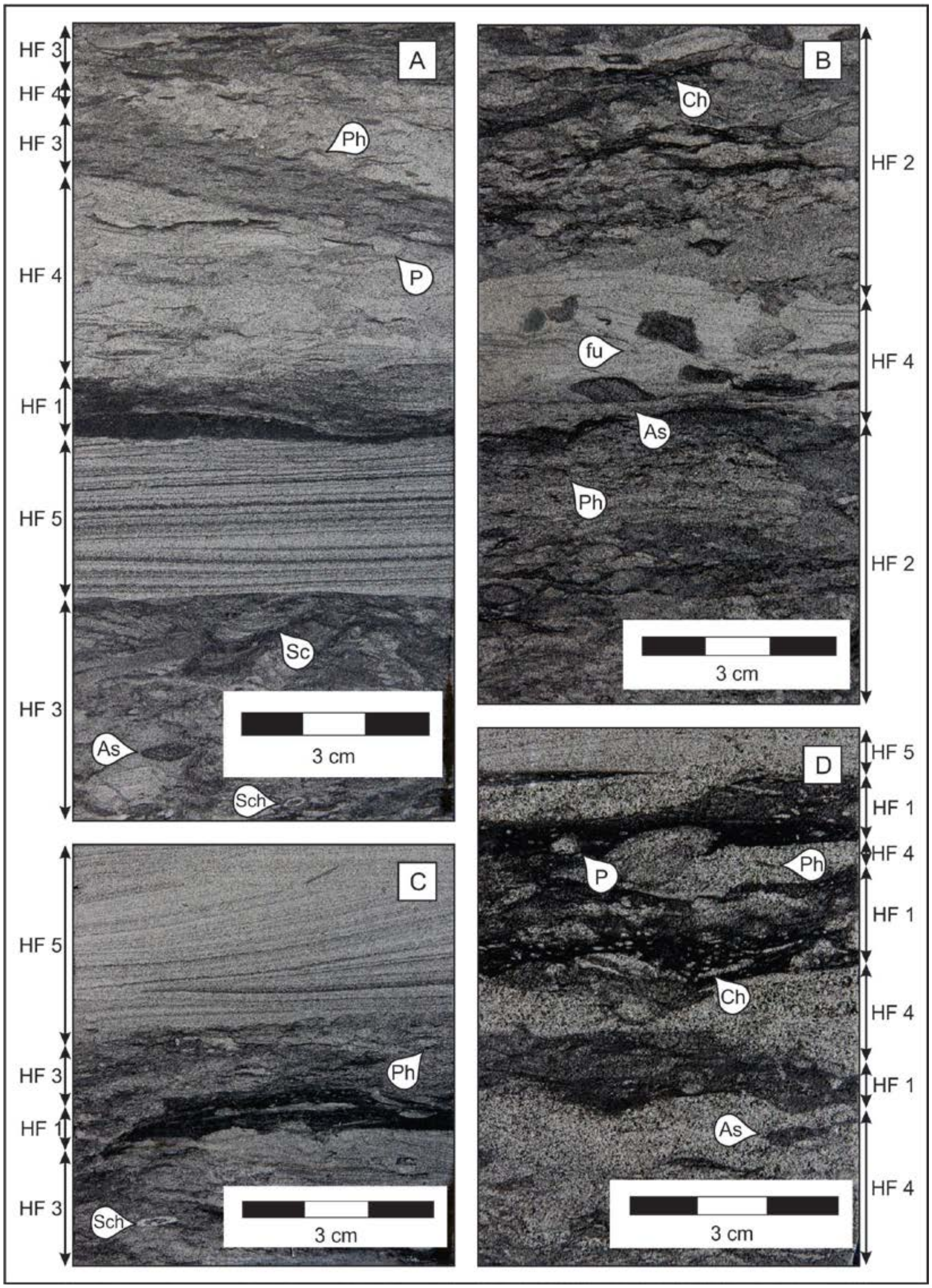
A
HF 3
HF 4
HF 3
HF 4
HF 1
HF 5
HF 3
Ph
P
Sc
As
Sch
3 cm
B
HF 2
HF 4
HF 2
Ch
fu
As
Ph
3 cm
C
HF 5
HF 3
HF 1
HF 3
Ph
Sch
3 cm
D
HF 5
HF 1
HF 4
HF 1
HF 4
HF 1
HF 4
P
Ph
Ch
As
3 cm

Figure 7 Examples of hydrofacies. A) Hydrofacies (HF) 3, 4, and 5 with *Phycosiphon* (Ph), *Planolites* (P), *Scolicia* (Sc), *Asterosoma* (As), and *Schaubcylindrichnus* (Sch). HF 5 exhibits planar parallel laminae. B) HF 2 with *Chondrites* (Ch), *Asterosoma* (As), and *Phycosiphon* (Ph) interbedded with laminated HF 4 containing *Asterosoma* (As) and fugichnia (fu). C) Wave ripple laminated HF 5 overlying HF 3 and HF 1. Trace fossils in HF 3 include *Phycosiphon* (Ph) and *Schaubcylindrichnus* (Sch). D) HF 5 and HF 4 interbedded with HF 1. Trace fossils in HF 4 include *Asterosoma* (As) and *Phycosiphon* (Ph). Trace fossils in HF 1 include *Planolites* (P) and *Chondrites* (Ch).

5.2 Transition Probability (Markov Chain) Analyses

The transition probability matrices are shown in Figure 8 for grain size vs. k_{max} and in Figure 9 for HF vs. k_{max}. The transitions from class 1 to 2 are read from rows to columns. The dominant control on permeability should have similar transition probability curves as k_{max}. The Markov chains for grain size (Figure 8) show similar transition probability trends only in column 1 and column 5. Units with clay-sized grains typically appear structureless, and the trace fossil suite observed within these units is dominated by mud-filled trace fossils. Units dominated by lower medium (mL)-grained sandstone typically lack bioturbation, and are structureless or laminated. This suggests that grain size only influences permeability where the rock units are relatively homogeneous, whereas intermediate permeabilities (i.e. 0.1-10 mD) are controlled by a number of variables captured by the hydrofacies. The k_{max} values were classed for the transition probability analyses to enable comparison of the two approaches.

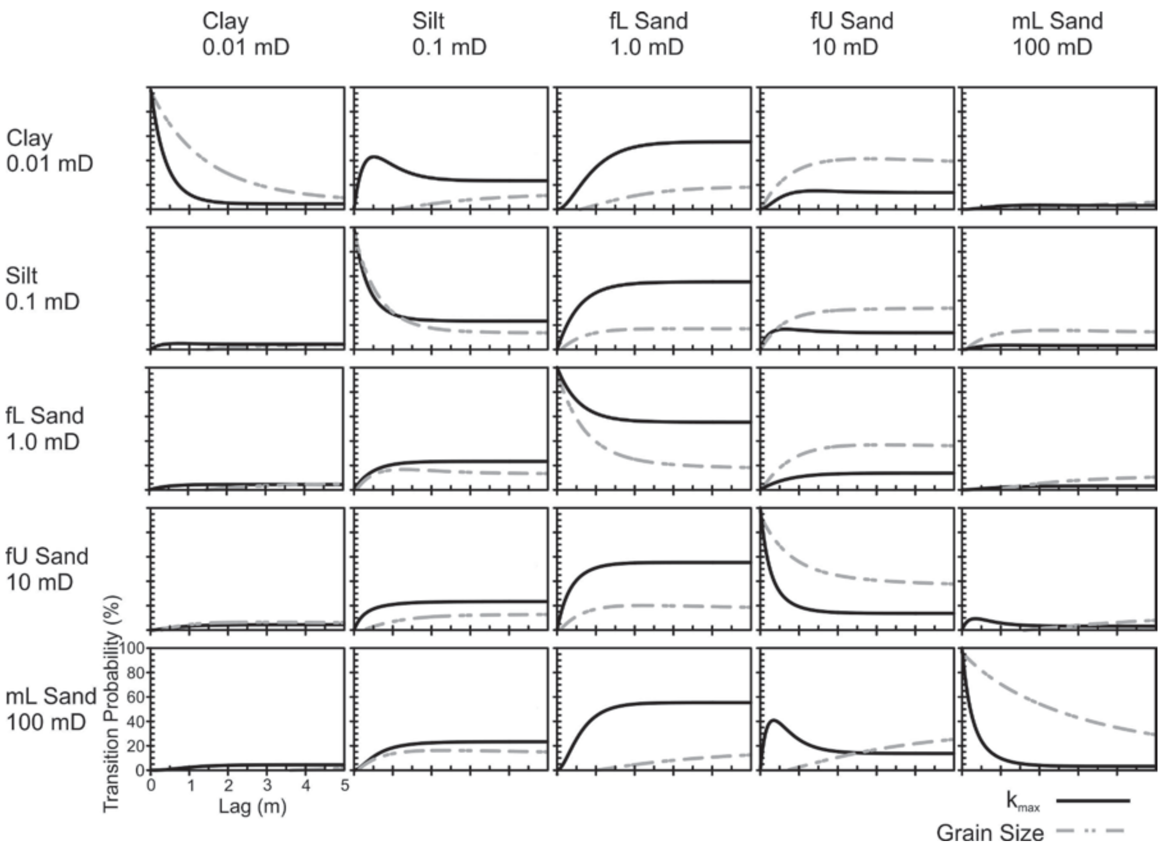

Figure 8 Vertical transition probability matrix for k_{max} (solid black line) vs. grain size (dashed gray line). fL: lower fine-grained; fU: upper fine-grained; mL: lower medium-grained.

The transition probability matrix for HF shows superior correspondence to k_{max} (Figure 9). The Markov chains show that transitions from one k_{max} class to another vertically down the well are closely related to transitions from one HF class to another. For example, the matrix shows that for column 2, the probability of k_{max} transitioning to

0.1 mD is similar to the probability of a particular HF transitioning to HF 2, which is a silty mudstone containing moderate proportions of interstitial silt and sand and generally high bioturbation intensities (BI 4-5). Core plug analyses show that HF 2 has a geometric average permeability of 0.35 mD, which is consistent with k_{max} class (0.1 mD) used in the transition probability analysis. The difference in transition rates between HF and k_{max} implies that their average bed thicknesses are different.

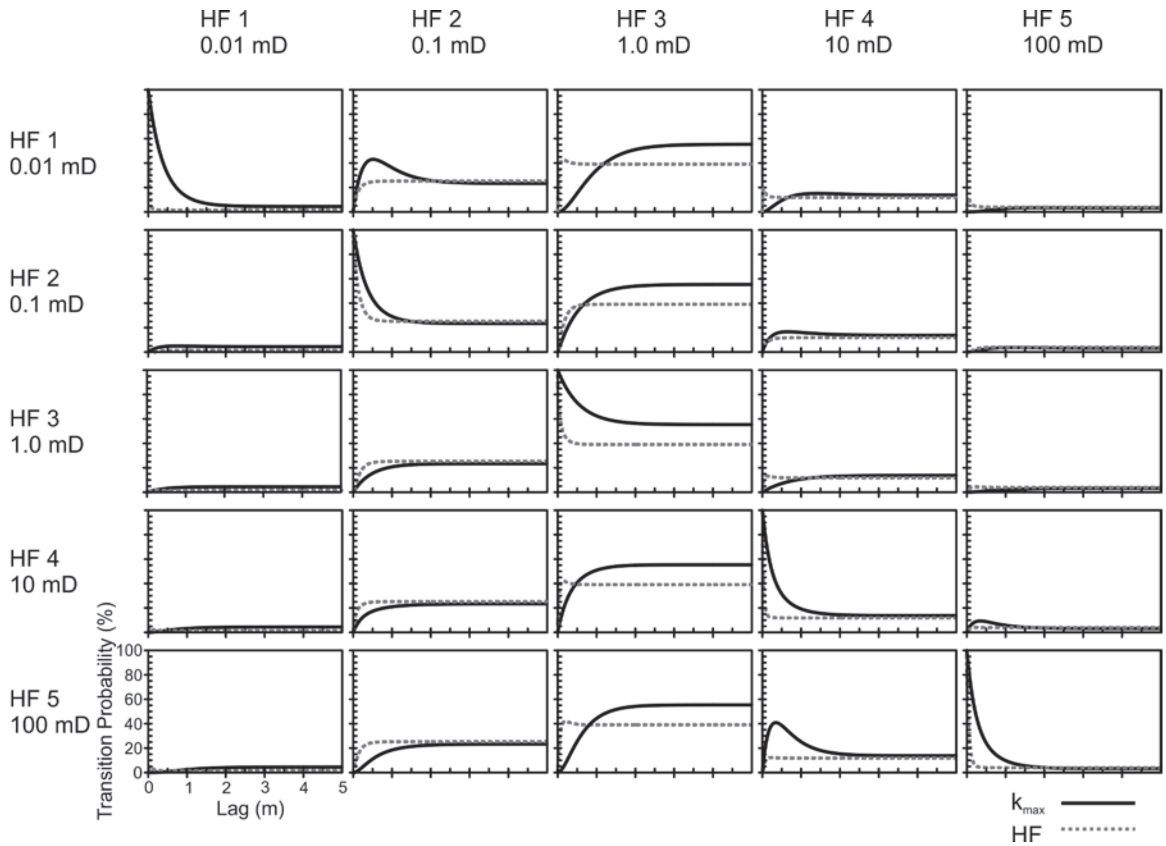

Figure 9 Vertical transition probability matrix for k_{max} (solid black line) vs. hydrofacies (dotted gray line).

The results of the Markov transition probability were also analyzed for correlation. A correlation of +100% indicates a perfect direct relationship between two variables, and a correlation of -100% indicates a perfect inverse relationship. A correlation of zero indicates a lack of correlation (Davis, 1986). The Markov chains show that the volumetric proportions, as indicated by the sill values of different k_{max} classes, correlate with grain size by 15%, even though it is commonly assumed that grain size and permeability have a high, positive correlation (coarse grain sizes being associated with high permeability). However, permeability correlates with the established hydrofacies by 97%, indicating that variations in permeability down the well are strongly related to variations in the HF.

6. Conclusions

The results from the transition probability analyses show that horizontal permeability does not correlate well with conventional grain size classifications alone, suggesting that permeability is controlled by additional factors, such as sedimentary structures, bioturbation, and sedimentary accessories. In the studied core intervals, bioturbation plays an important role in the creation and alteration of permeable flow paths within these fine-grained units by generating sand-filled burrows and destroying primary sedimentary structures. Therefore, in order to show a consistent correlation between rock type and permeability, it is important to characterize the rock on the basis of all of its physical, chemical, biogenic, and hydraulic properties by defining the hydrofacies. These hydrofacies show a clear and quantifiable relationship to permeability in the vertical direction. The results show that in the studied well, grain size only correlates closely to permeability in homogeneous, very coarse- or very fine-grained rock units such as sandstone (HF 5) or mudstone (HF 1). In contrast, the transiograms for HF show similar sill values with k_{max}, indicating that the two attributes have comparable volumetric proportions within the cored interval. Nevertheless, the difference in transition rates between HF and k_{max} indicates that their average bed thicknesses are different.

The T-PROGS software used for the transition probability calculations limits the geologic data to a maximum of five different classes, which may be insufficient to adequately represent some geologically complex reservoirs. Other limitations to this study include the small number of permeability values for the studied cored interval. Only horizontal k_{max} values were available for the transition probability analysis. Additionally, permeability measurements are historically only conducted on the coarsest-grained units, despite the fact that these facies types may not be representative of the dominant flow unit in tight reservoirs. The paucity of permeability analyses in muddy or strongly heterolithic bedsets limits the applicability of statistical analyses. Micropermeametry may be used to refine the k_{ave} of each HF, as it measures detailed and precise permeability at the centimetre scale. Nonetheless, the approach for defining hydrofacies is directly applicable to all low-permeability reservoirs, wherein grain size may not be the dominant factor but rather only one of many controls on permeability distributions. This approach can potentially be used as a conceptual framework for the spatial modeling of permeability in low-permeability reservoirs.

Acknowledgments

The authors wish to thank Mike Ranger for the use of AppleCORE®. We would also like to thank Andrew La Croix for his assistance in core logging, and Kevin Gillen for his assistance in the analyses of permeability data. The paper benefited from the review of Dr. Dirk Knaust and suggestions by Associate Editor Dr. Luis Buatois. Dr. Richard Lockhart and Dr. Derek Bingham are thanked for their helpful insights on transition probability analyses. This research was supported by Natural Sciences and Engineering Research Council (NSERC) Discovery Grants to James MacEachern and Diana Allen.

References

AccuMap IHS. Available from: http://www.ihs.com/products/oil-gas-information/analysis-software/accumap/index.aspx. Accessed 06 February 2013.

Beaumont, E.A., 1984. Retrogradational shelf sedimentation: Lower Cretaceous Viking Formation, central Alberta. In: Tillman, R.W., and Siemers, C.T. (Eds.). Siliciclastic Shelf Sediments. SEPM Special Publication 34, pp. 163-177.

Bloch, J., Schröder-Adams, C., Leckie, D.A., McIntyre, D.J., Craig, J., and Staniland, M., 1993. Revised stratigraphy of the lower Colorado Group (Albian to Turonian), Western Canada: Bulletin of Canadian Petroleum Geology 41, 325-348.

Boreen, T. and Walker, R.G., 1991. Definition of allomembers and their facies assemblages in the Viking Formation, Willesden Green area, Alberta. Bulletin of Canadian Petroleum Geology 39, 123-144.

Burton, J.A. and Walker, R.G., 1999. Linear transgressive shoreface sandbodies controlled by fluctuations of relative sea level: Lower Cretaceous Viking Formation in the Joffre-Mikwan-Fenn area, Alberta, Canada. In: Bergman, K.M., and Snedden, J.W. (Eds.). Isolated Shallow Marine Sand Bodies: Sequence Stratigraphic and Sedimentologic Perspectives. SEPM, Special Publications 64, pp. 255-272.

Cahn, M.D., Hummel, J.W., and Brouer, B.H., 1994. Spatial-analysis of soil fertility for site-specific crop management. Soil Science Society of America Journal 58, 1240-1248.

Caldwell, W.G.E., 1984. Early Cretaceous transgressions and regressions in the southern Interior Plains. In: Stott, D.F., and Glass, D.J. (Eds.). The Mesozoic of Middle North America. Canadian Society of Petroleum Geologists, Memoir 9, pp. 173-203.

Caldwell, W.G.E., Diner, R., Eicher, D.L., Fowler, S.P., North, B.R., Stelck, C.R. and von Holdt Wilhelm, L., 1993. Foraminiferal biostratigraphy of Cretaceous marine cyclothems. *In:* Evolution of the Western Interior Basin. Caldwell, W.G.E. and Kauffman, E.G. (Eds.) Geological Association of Canada, Special Paper 39, pp. 477-520.

Carle, S.F., 1999. T-PROGS: Transition Probability Geostatistical Software. Version 2.1 User's Guide. University of California, Davis, CA.

Clarkson, C. and Pedersen, P., 2010. Tight oil production analysis: Adaptation of existing rate-transient analysis techniques. Society of Petroleum Engineers Paper 137352 Presented at the Canadian Unconventional Resources and International Petroleum Conference, Calgary, Alberta.

Cobban, W.A. and Kennedy, W.J., 1989. The ammonite *Metengonoceras* Hyatt, 1903, from the Mowry Shale (Cretaceous) of Montana and Wyoming. United States Geological Survey Bulletin 1787-L, pp. L1-L11.

Cunningham, K.J., Sukop, M.C., Huang, H., Alvarez, P.F., Curran, H.A., Renken, R.A., and Dixon, J.F., 2009. Prominence of ichnologically influenced macroporosity in the karst Biscayne aquifer: Stratiform 'super-K' zones. GSA Bulletin 121, 164-180.

Davis, J.C., 1986. Statistics and data analysis in geology. John Wiley & Sons, New York, pp. 38.

Dewhurst, D.N., Aplin, A.C., and Sarda, J.P., 1999. Influence of clay fraction on pore-scale properties and hydraulic conductivity of experimentally compacted mudstones. Journal of Geophysical Research 104, 29261-29274.

Dewhurst, D.N., Aplin, A.C., Sarda, J.P., and Yang, Y.L., 1998. Compaction-driven evolution of porosity and permeability in natural mudstones: An experimental study. Journal of Geophysical Research 103, 651-661.

Dornbos, S.Q., Phelps, W., Bottjer, D.J., Droser, M.L., and Anderson, B., 2000. Effects of bioturbation on reservoir sandstone porosity and permeability: Studies of outcrop samples from the upper Cretaceous, Book Cliffs, Utah (abs.). AAPG Annual Meeting Program 9, A40.

Gingras, M.K., Baniak, G., Gordon, J., Hovikoski, J., Konhauser, K.O., La Croix, A., Lemiski, R., Mendoza, C., Pemberton, S.G., Polo, C., and Zonneveld, J.P., 2012. Porosity and permeability in bioturbated sediments. *In* Trace Fossils as Indicators of Sedimentary Environments. *Edited by* D. Knaust and R.G. Bromley. Developments in Sedimentology 64, pp. 835-868.

Gingras, M.K., Mendoza, C.A., and Pemberton, S.G., 2004. Fossilized worm burrows influence the resource quality of porous media. AAPG Bulletin 88, 875-883.

Glaister, P., 1959. Lower Cretaceous of southern Alberta and adjoining areas. American AAPG Bulletin 43, 590-640.

Grinstead, C.M. and Snell, J.L., 1997. Introduction to probability. American Institute of Mathematics, Palo Alto, pp. 405-413.

Haq, B.U., Hardenbol, J., and Vail, P.R., 1987. Chronology of fluctuating sea levels since the Triassic. Science 235, 1156-1177.

Holditch, S.A., 2006. Tight gas sands. Journal of Petroleum Technology 58, 86-93.

Hovikoski, J., Pemberton, S.G., Gingras, M.K., Lemiski, R., and Olexson, R., 2007. Effect of bioturbation in low permeability gas charged reservoirs-a case study from the upper Cretaceous Milk River Fm., western Canada (abs.). AAPG Annual Convention and Exhibition, pp. 66-67.

Jones, N.L., Walker, J.R., and Carle, S.F., 2002. Using transition probability geostatistics with MODFLOW. IAHS Publication 277, 359-364.

Kauffman, E.G., 1977. Geological and biological overview: Western Interior Cretaceous Basin. In: Kauffman, E.G. (Ed.). Cretaceous Facies, Faunas, and Paleoenvironments across the Western Interior Basin. Rocky Mountain Association of Geologists 14, pp. 75-99.

Knaust, D., 2014. Classification of bioturbation-related reservoir quality in the Khuff Formation (Middle East): towards a genetic approach. In: Pöppelreiter, M.C. (Ed.). Permo-Triassic Sequence of the Arabian Plate. EAGE, pp. 247-267.

La Croix, A.D., Gingras, M.K., Pemberton, S.G., Mendoza, C.A., MacEachern, J.A., and Lemiski, R.T., 2013. Biogenically enhanced reservoir properties in the Medicine Hat gas field, Alberta, Canada. Marine and Petroleum Geology 43, 464-477.

Leckie, D.A., Staniland, M.R., and Hayes, B.J., 1990. Regional maps of the Albian Peace River and lower Shaftsbury formations on the Peace River Arch, northwestern Alberta and northeastern British Columbia. Bulletin of Canadian Petroleum Geology 38A, 176-189.

Lemiski, R.T., Hovikoski, D.J., Pemberton, S.G., and Gingras, D.M., 2011. Sedimentological ichnological and reservoir characteristics of the low-permeability, gas-charged Alderson member (Hatton gas field, southwest Saskatchewan): Implications for resource development. Bulletin of Canadian Petroleum Geology 59, 27-53.

Li, W.D., Zhang, C.R., Burt, J.E., and Zhu, A.X., 2005. A Markov chain-based probability vector approach for modeling spatial uncertainties of soil classes. Soil Science Society of America Journal 69, 1931-1942.

Long, D., 1979. Geotechnical results from BH78/11. St. Magnus Bay, Shetland. British Geological Survey, Edinburgh, BGS, Report 79/17.

Long, D. and Hobbs, P.R.N., 1979. Geotechnical properties of sediments from the borehole 77/75 (North Sea). British Geological Survey, Edinburgh, BGS, Report 79/4.

MacEachern, J.A. and Bann, K.L., 2008. The role of ichnology in refining shallow marine facies models. In: Hampson, G., Steel, R., Burgess, P., and Dalrymple, R. (Eds.). Recent Advances in Models of Siliciclastic Shallow-Marine Stratigraphy. SEPM Special Publication 90, pp. 73-116.

MacEachern, J.A., Zaitlin, B.A., and Pemberton, S.G., 1999. A sharp-based sandstone of the Viking Formation, Joffre field, Alberta, Canada: Criteria for recognition of transgressively incised shoreface complexes. Journal of Sedimentary Research 69, 876-892.

McDowell, R.R., Matchen, D.L., and Avary, K.L., 2001. Bioturbation and reservoir flow characteristics: where did the permeability go? Annual Meeting Expanded Abstracts, AAPG 85, 131.

McGookey, D.P., Haun, J.D., Hale, L.A., Goodell, H.G., McCubbin, D.G., Weimer, R.J., and Wulf, G.R., 1972. Cretaceous System. In: Mallory, W.W. (Ed.), Geological Atlas of the Rocky Mountain Region, U.S.A. Rocky Mountain Association of Geologists, Denver Colorado, pp. 190-228.

Mesri, G. and Olson, R.E., 1971. Mechanisms controlling the permeability of clays. Clays and Clay Minerals 19, 151-158.

Nagaraj, T.S., Pandian, N.S., and Narasimha Raju, P.S.R., 1994. Stress-state permeability relations for overconsolidated clays. Geotechnique 44, 349-352.

Obradovich, J., 1993. A Cretaceous time scale. In: Caldwell, W.G.E., and Kauffman, E.G. (Eds.), Evolution of the Western Interior Basin. Geological Association of Canada Special Paper 39, pp. 379-396.

Pattison, S., 1991. Sedimentology and allostratigraphy of regional, valley-fill, shoreface and transgressive deposits of the Viking Formation (Lower Cretaceous), central Alberta. PhD. Thesis, School of Geography and Earth Sciences, McMaster University, Hamilton, Ontario, 380p.

Pemberton, S.G. and Gingras, M.K., 2005. Classification and characterizations of biogenically enhanced permeability. AAPG Bulletin 89, 1493-1517.

Posamentier, H.W. and Chamberlain, C.J., 1993. Sequence stratigraphic analysis of Viking Formation lowstand beach deposits at Joarcam field, Alberta, Canada. In: Posamentier, H.W., Summerhayes, C.P., Haq, B.U., and Allen, G.P. (Eds.), Stratigraphy and Facies Associations in a Sequence Stratigraphic Framework. International Association of Sedimentologists, Special Publication 18, pp. 469-485.

Qi, Y., 1998. Relations between bioturbation structures and petrophysical properties of Donghe sandstone reservoirs in central Tarim. Oil and Gas Geology 4, 318-320.

Qi, Y., Hu, B., and Zhang, G., 2000. The influence of bioturbation structures containing *Ophiomorpha* on petrophysical properties of Donghe sandstone reservoir in central Tarim Basin, China (abs.). 31st International Geological Congress.

Raychaudhuri, I. and Pemberton, S.G., 1992. Ichnological and sedimentological characteristics of open marine to storm-dominated restricted marine settings within the Viking/Bow Island formations, south-central Alberta. Applications of Ichnology to Petroleum Exploration. SEPM Core Workshop 17, 119-139.

Reineck, H.E. 1963. Sedimentgefûge im Bereich der sûdlichen Nordsee: Senckenbergische Naturforschende Gesellschaft, Abhandlungen, 505p.

Reinson, G.E., Warters, W.J., Cox, J., and Price, P.R., 1994. Chapter 21: Cretaceous Viking formation of the western Canada sedimentary basin. In: Mossop, G.D., and Shetsen I. (Eds.). Geological Atlas of the Western Canada Sedimentary Basin. Canadian Society of Petroleum Geologists and Alberta Research Council, pp. 353-363.

Spencer, C.W., 1989. Review of characteristics of low-permeability gas reservoirs in western United States. AAPG Bulletin 73, 613-629.

Stelck, C.R., 1958. Stratigraphic position of the Viking sand. Bulletin of Canadian Petroleum Geology 6, 2-7.

Stelck, C.R. and Koke, K.R., 1987. Foraminiferal zonation of the Viking interval in the Hasler Shale (Albian), northeastern British Columbia. Canadian Journal of Earth Sciences 24, 2254-2278.

Stelck, C.R. and Leckie, D.A., 1990. Biostratigraphy of the Albian Paddy Member (Lower Cretaceous Peace River Formation), Goodfare, Alberta. Canadian Journal of Earth Sciences 27, 1159-1169.

Taylor, A.M. and Goldring, R., 1993. Description and analysis of bioturbation and ichnofabric. Journal of the Geological Society 150, 141-148.

Taylor, A.M., Goldring, R., and Gowland, S., 2003. Analysis and application of ichnofabrics. Earth Science Reviews 60, 227-259.

Tonkin, N.S., McIlroy, D., Meyer, R., and Moore-Turpin, A., 2010. Bioturbation influence on reservoir quality: A case study from the cretaceous Ben Nevis formation, Jeanne d'Arc basin, offshore Newfoundland, Canada. AAPG Bulletin 94, 1059-1078.

Vail, P.R., Mitchum, R.M., and Thompson, S., 1977. Seismic stratigraphy and global changes of sea level. In: Payton, C.E. (Ed.). Seismic Stratigraphy—Applications of Hydrocarbon Exploration. American Association of Petroleum Geologists, Memoir 26, pp. 83-97.

Volkenborn, N., Polerecky, L., Hedtkamp, S.I.C., van Beusekom, J.E.E., and de Beer, D., 2007. Bioturbation and bioirrigation extend the open exchange regions in permeable sediments. Limnology and Oceanography 52, 1898-1909.

Walker, R.G., 1990. Facies modeling and sequence stratigraphy. Journal of Sedimentary Petrology 60, 777-786.

Walker, R.G., 1995. Sedimentary and tectonic origin of a transgressive surface of erosion: Viking Formation, Alberta, Canada. Journal of Sedimentary Research Section B-Stratigraphy and Global Studies 65, 209-221.

Weimer, R.J., 1984. Relation of unconformities, tectonics and sea-level changes, Cretaceous of Western Interior, U.S.A. In: Schlee, J.S. (Ed.). Interregional Unconformities and Hydrocarbon Accumulation. American Association of Petroleum Geologists, Memoir 36, pp. 7-35.

Weissmann, G.S., 2005. Application of transition probability geostatistics in a detailed stratigraphic framework. *In* Workshop for GSA Annual Meeting, Three-dimensional geologic mapping for groundwater applications, University of New Mexico, USA, pp. 105-108.

Wentworth, C.K., 1922. A scale of grade and class terms for clastic sediments. Journal of Geology 30, 377-392.

Williams, G.D. and Stelck, C.R., 1975. Speculations on the Cretaceous paleogeography of North America. In: Caldwell, W.G.E. (Ed.). The Cretaceous System in the Western Interior of North America. Geological Association of Canada Special Paper 13, pp. 1-20.

Yang, Y. and Aplin, A.C., 2007. Permeability and petrophysical properties of 30 natural mudstones. Journal of Geophysical Research 112, B03206.

Yang, Y. and Aplin, A.C., 2010. A permeability–porosity relationship for mudstones. Marine and Petroleum Geology 27, 1692-1697.